Foreign object damage and fatigue crack threshold: Cracking outside shallow indents

XI CHEN and JOHN W. HUTCHINSON
Division of engineering and applied sciences, Harvard university, Cambridge, MA 02138, USA

Abstract. Foreign Object Damage (FOD) usually happens when objects are ingested into jet engines powering military or civil aircraft. Under extreme conditions, FOD can lead to severe structural damage. More commonly it produces local impacted sites of the fan and compressor airfoils, lowering fatigue life of these components. FOD is a prime cause for maintenance and repair in aircraft engines. In this paper, a framework for analyzing FOD and its effect on fatigue cracking is established. A finite element analysis is used to identify three relevant regimes of FOD related to the depth of penetration into the substrate, and to determine the residual stresses. Most of the emphasis in this paper focuses on fatigue cracks emerging from shallow indentations, which are generally expected to be of most practical concern. Full three-dimensional finite element solutions are obtained for semicircular surface cracks emerging from specific locations at the indentation revealing the influence of the residual stress on the stress intensity factor distribution. For shallow indents, a relatively simple dimensionless formula for the relation between the residual stress intensity factor, the crack size, and the indentation width are developed. These results, together with results for the intensity factor variations due to cyclic loading, have been used to address the question: To what extent do the residual stresses caused by the FOD reduce the critical crack size associated with threshold fatigue crack growth? Formulas for the critical crack size are obtained. Specific results are presented for the blade alloy, Ti-6Al-4V, revealing that FOD can reduce the critical crack size by as much as 60%.

Key words: Foreign object damage, contact mechanics, crack mechanics, fatigue analysis, indentation regimes, critical crack size.

1. Introduction

Foreign object damage by hard-particles mainly occurs during motion of the aircraft on the airfield, during takeoff and during landing. Typical objects ingested are stones and other debris from the airfield, with sizes in the millimeter regime. Typical impact velocities are in the range of 100 - 350 m/s, depending on the specific engine. Of concern here are impact locations on the blades. Such microstructural damage can promote fatigue-crack growth under high-cycle fatigue loading. This has become a critical issue in the lifetime prediction of turbine-engine components and a prime concern in maintenance and repair (Ritchie et al., 1999; Peters et al., 2000). The unusually high frequencies typical of in-flight vibratory loading necessitate a defect-tolerant approach based on designing below the threshold for fatigue crack propagation. FOD damage must be factored into this approach. Otherwise, the FOD damage can lead to non-conservative life prediction and unexpected high-cycle fatigue failures.

Most FOD occur as damage to the leading edges of turbine blades. To gain insight into the interaction between FOD and fatigue cracking, we have considered a less frequent form of FOD whereas the damage is assumed to occur away from the edge. The research has been coordinated with a parallel experimental study (Peters et al., 2000). The study initiated in
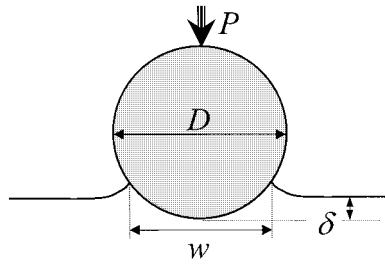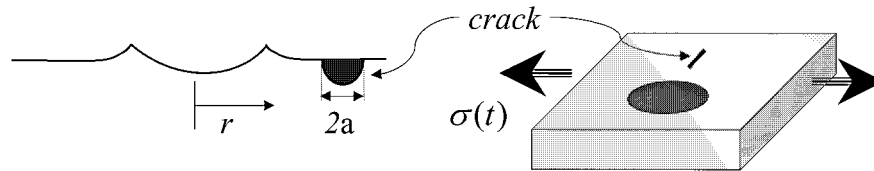
Figure 1. The geometry of spherical indentation.

Figure 2. A semi-circular surface crack with radius *a* is embedded inside the residual stress field of the indent and subjected to cyclic stress $\sigma(t)$.

this paper considers the normal impression of a hard spherical particle into a thick elastic-plastic substrate (Figure 1). The indentation field is axisymmetric. The resulting residual stresses are determined and the locations at the surface where tensile stresses are most likely to promote cracking are identified. The second step in the approach is the three-dimensional finite element analysis of a semi-circular surface crack within the residual stresses field. The final step combines the stationary stress intensity factor due to the indent with the intensity factor variation due to the cyclic loads (Figure 2) to make predictions for critical crack sizes based on threshold fatigue crack growth data.

The parallel experimental study has been conducted by Peters et al. (2000), who investigated the influence of FOD on the high-cycle fatigue properties of Ti-6Al-4V alloy, which is commonly used as gas turbine blades in military aircraft. The material is almost ideally plastic with very little strain hardening and a tensile yield stress of about 950 MPa. In their experiments, they used hardened steel spheres (with diameter 3.175 mm) to normally impact a flat Ti-6Al-4V alloy specimen at 200–300 m s^{-1}. After impact, the specimens were cycled at a maximum nominal stress of 500 MPa at a load ratio of 0.1, and the initiation and subsequent growth of the fatigue cracks emerging from the indent were observed. The authors found that FOD provides sites for the initiation of small fatigue cracks, and in some cases crack initiation occurred at cycle lifetimes which were orders of magnitude lower than found for un-impacted specimens. For the 200 m s^{-1} impact, crack initiation was observed to occur at the bottom of the indent, while the 300m/s impact a prominent crater rim was produced and this turned out to be the site of the crack initiation.

The paper is organized by sections to follow the three steps mentioned in connection with the overall approach. Section 2 presents the indentation analysis and results. Here contact is made with recent work on the finite element analysis of indentation. In particular, it will be seen that three separate regimes to the indentation problem can be identified: very shallow, moderately shallow and deep indents. The primary focus in this paper will be on moderately shallow indents for which relatively simple scaling relations exist for the residual stress fields. Some discussion of trends for deep indentations will also be given. The solutions for the stress intensity factor for a semi-circular surface crack within the residual stress field of the
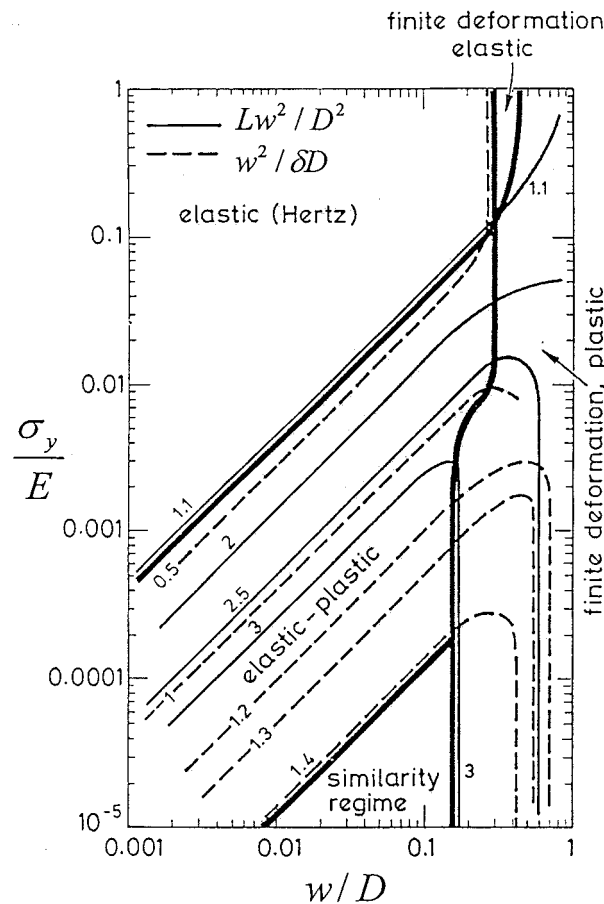
Figure 3. The indentation map from Mesarovic and Fleck (1999a).

indent are presented in Section 3. Finally, in Section 4, the stress intensity factor history accounting for both residual stresses and cyclic loads is assembled and used to predict the largest crack size such that the growth rate is below threshold using data for the Ti-6Al-4V alloy. An analytical method is developed in Section 4 and its accuracy is examined in the next section with full finite element solutions. Some further discussions on the limiting crack radius are also addressed in Section 5. The main findings of this paper are summarized in the last section.

2. Residual stresses arising from indentation

As depicted in Figure 1, a rigid sphere of diameter D is pushed into a half-space to by a load P. The indentation load is then removed such that the contact diameter is w and the indent depth is δ, both measured after unloading. The material is taken to be elastic-ideally plastic with tensile yield stress σ_y, Young's modulus E and Poisson's ratio ν. This representation is realistic for the titanium alloy Ti-6Al-4V, which has little strain hardening (Ritchie et al., 1999). The half-space is taken to be initially stress-free and infinitely deep, consistent with the assumption that the foreign object is small compared to the substrate thickness. The work

of Mesarovic and Fleck (1999a) reveals that the Poisson's ratio of the substrate material is a minor factor in indentation.

Johnson's classical book (Johnson, 1985) on theoretical contact mechanics contains considerable discussion and modeling of the Brinell's indentation test wherein a stiff elastic sphere is pushed into the surface of an elastic-plastic solid. The load per unit area of impression defines the hardness and is used as a measure of resistance of the material to plastic flow. For the most part, the results in Johnson's book do not reflect the most recent progress in indentation analysis made possible by today's advanced finite element methods. A recent comprehensive finite element study by Mesarovic and Fleck (1999a, 1999b) serves to set the stage for the present problem. Specifically, Mesarovic and Fleck have considered precisely the same indentation problem stated above, but with emphasis on hardness prediction and no determination of residual stresses which are of primary interest here. They show that there are various distinct regimes to the indentation problem. Their indentation regime map is given in Figure 3. Briefly, at sufficiently high and low the response is elastic and characterized by the classical Hertz solution. At a given , plasticity becomes increasingly important as increases. For greater than about 0.16, finite strain effects (large strains and large rotations) begin to become dominant. This corresponds to the regime referred to here as deep indentation. For smaller than 0.16, small strain kinematics pertain. This regime, as it will be seen, sub-divides into two parts, named here as very shallow and moderately shallow indentations, with distinctly different residual stress fields. The regime of primary interest in this paper is that of moderately shallow indentations. Included in the map of Mesarovic and Fleck is a 'similarity regime' characterized by relatively simple functional scaling of the solution as developed by Hill et al. (1989), Bower et al. (1993) and Biwa et al. (1995). This sector of the map lies outside the range of practical concern for the applications in the present study. Mesarovic and Fleck also found that the boundaries of the various indentation regimes are relatively insensitive to the degree of strain hardening and to the level of interfacial friction. However, the level of friction strongly affects the field beneath the indentor. A pre-stress within the half-space parallel to the free surface was shown to have a minor effect on the indentation response.

2.1. Very shallow, moderately shallow and deep indentations

From dimensional analysis, the residual stress distribution in the half-space after unloading can be written in the functional form

$$\frac{\sigma_{ij}(r,z)}{\sigma_y} = f_{ij}\left(\frac{P}{\frac{\pi}{4}D^2\sigma_y}, \frac{\sigma_y}{E}, \mu, \frac{r}{\sqrt{P/\sigma_y}}, \frac{z}{\sqrt{P/\sigma_y}}\right), \tag{1}$$

where e and z are the coordinates in the radial and axial direction, respectively, and μ is the Coulomb friction coefficient. Throughout, the dimensionless load factor will be denoted by

$$L \equiv \frac{P}{\frac{\pi}{4}D^2\sigma_y}. \tag{2}$$

The coordinates could be scaled by D, but the alternative choice in (1) is preferred in the regime of primary interest for moderately shallow indentations, as will be seen.

For given L, σ_y/E and μ (with $\nu = 0.3$) the stress distributions as functions of the dimensionless coordinates listed above have been computed. Finite element calculations were performed using the commercial code ABAQUS version 5.7 (Hibbit et al., 1998). The rigid
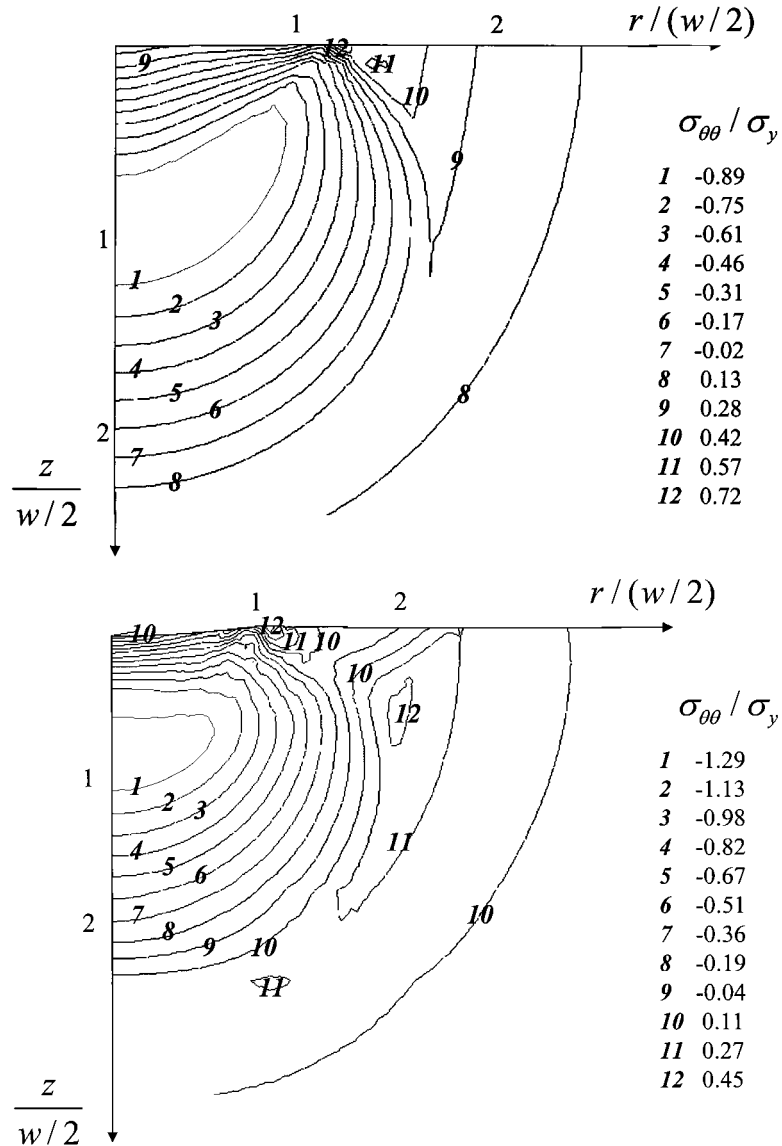
Figure 4. Residual hoop stress field due to indentation. (a) $L = 0.0013$, (b) $L = 0.064$, (c) $L = 1.91$.

contact surface option was used to simulate the rigid indentor, and the option for finite deformation and strain was employed. A typical mesh for the axis-symmetric indentation model comprises more than 2700 8-node elements. As already mentioned, the substrate material is taken to be elastic-perfectly plastic, with a Von Mises surface to specify yielding. Coulomb friction is invoked in the calculations, but it will be shown later that the choice of has only a minor influence on the stresses of interest in the FOD problem.

To make contact with the regime map in Figure 3, consider a representative substrate with $\sigma_y/E = 0.001$. If the Mesarovic–Fleck results are expressed in terms of L, one finds that the indentation is Hertzian for $L < 10^{-5}$; elastic-plastic but shallow if $10^{-5} < L < 0.08$, and is deep when $L > 0.08$. Figure 4 display the distributions of normalized residual hoop stress, $\sigma_{\theta\theta}/\sigma_y$, for three different load levels: very shallow, $L = 0.0013$; moderately shallow,
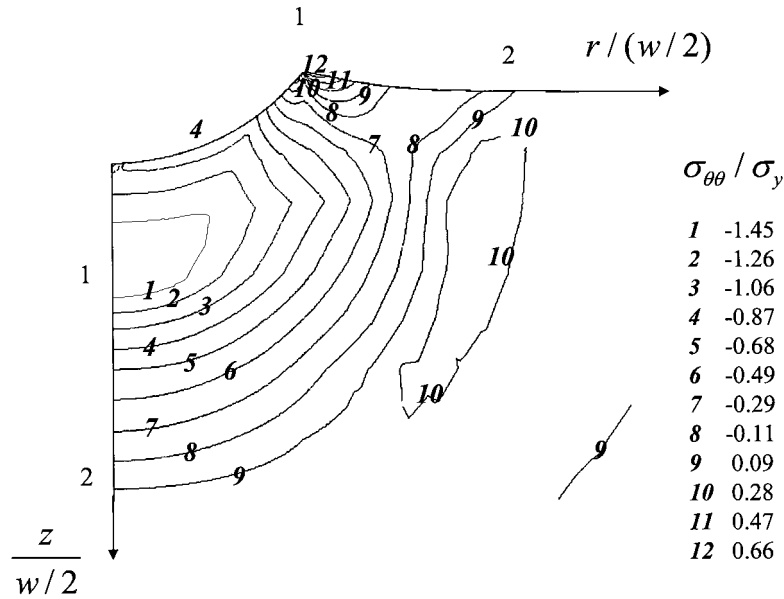
Figure 4. Continued.

$L = 0.064$; and deep, $L = 1.91$. These results were computed using and $\mu = 0.1$. In the very shallow regime (Figure 4a), the residual hoop stress within the indent is compressive or nearly so, but becomes tensile just outside the rim and then decays fairly rapidly to zero. For moderately shallow indents (Figure 4b), the surface hoop stress is tensile at the bottom of the indent, but becomes compressive just below the surface. Outside the rim, at a radius about twice that of the indent, the stress is tensile and extends to a considerable distance below the surface. The deep indent in Figure 4c displays compression within the indent and a pronounced tensile region just outside the rim. Then with increasing distance from the rim, the hoop stress becomes compressive and finally tensile again before decaying to zero. These trends are revealed by the plot in Figure 5 of as a function of L for points at the center of the indent, just outside the rim and a radius that is 2.2 times the rim radius. Figure 5 brings out the fact that the hoop stress outside the rim of the indent is essentially independent of L in the moderately shallow regime, which for $\sigma_y/E = 0.001$ corresponds to $0.006 < L < 0.4$. In this paper, we will focus on radial surface cracks lying outside the rim in the region of tensile hoop stress, primarily, but not exclusively, for moderately shallow indents. In subsequent work, we will address the problems for cracks at the center of the indent and cracks at the rim.

In experiments on fatigue cracks at FOD sites, radial cracks are observed but circumferential cracks are not. This is consistent with the residual stress calculations for the radial stress component, σ_{rr}, which is found to be weakly tensile only within the indent and then only very near to the surface. Thus, the focus in this paper, as mentioned, will be on radial cracks within regions of tensile hoop stress. A somewhat different cracking pattern is observed in thin brittle, elastic films bonded to metal substrates, which are then impressed by a spherical indenter (Begley et al., 1999). In this case, the predominant tensile stress in the elastic film is the radial component within the indent. Closely spaced cracks in the film are observed to form running circumferentially around the indent.
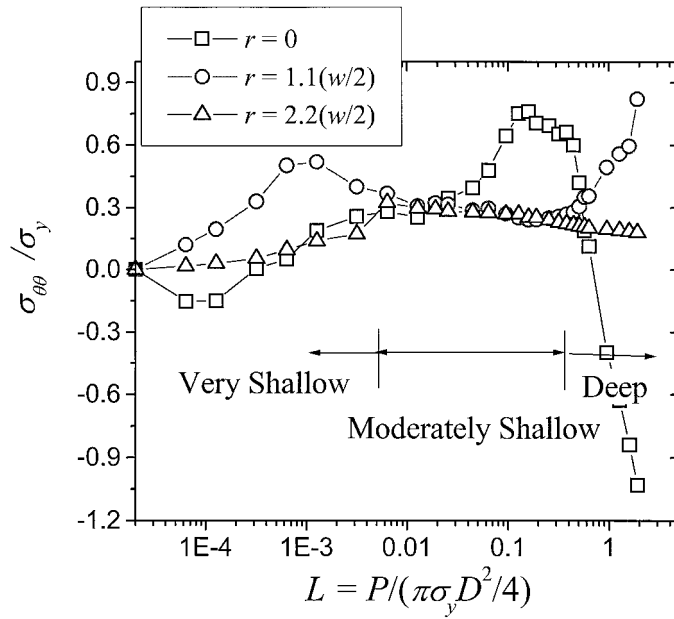
Figure 5. The normalized residual surface hoop stress $\sigma_{\theta\theta}/\sigma_y$ as a function of L at three locations. Identification of the three indentation regimes.

2.2. SCALING RELATIONSHIPS FOR MODERATELY SHALLOW INDENTS

In order to display the stress behavior in the regime of moderately shallow indentation from another angle, plots of normalized hoop stress at the surface as a function of r/w are given in Figure 6 for four L values at the lower end of the regime. The emphasis here is on behavior
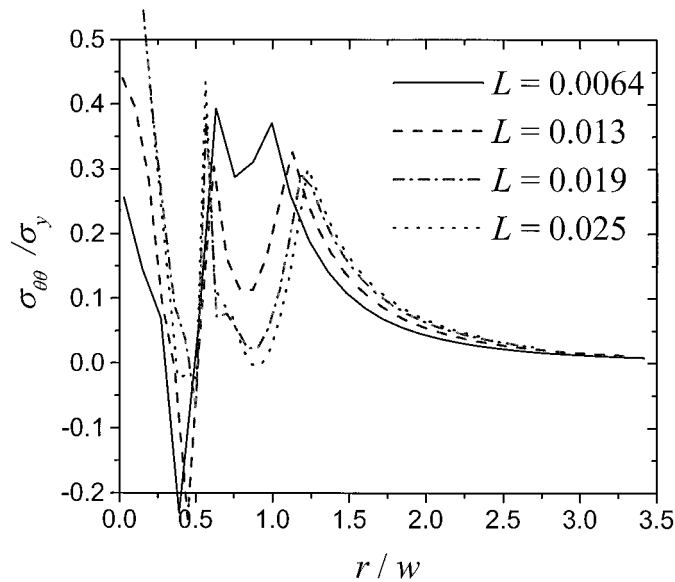

Figure 6. The relation between surface hoop stress $\sigma_{\theta\theta}/\sigma_y$ and r/w for loads within the moderately shallow regime.
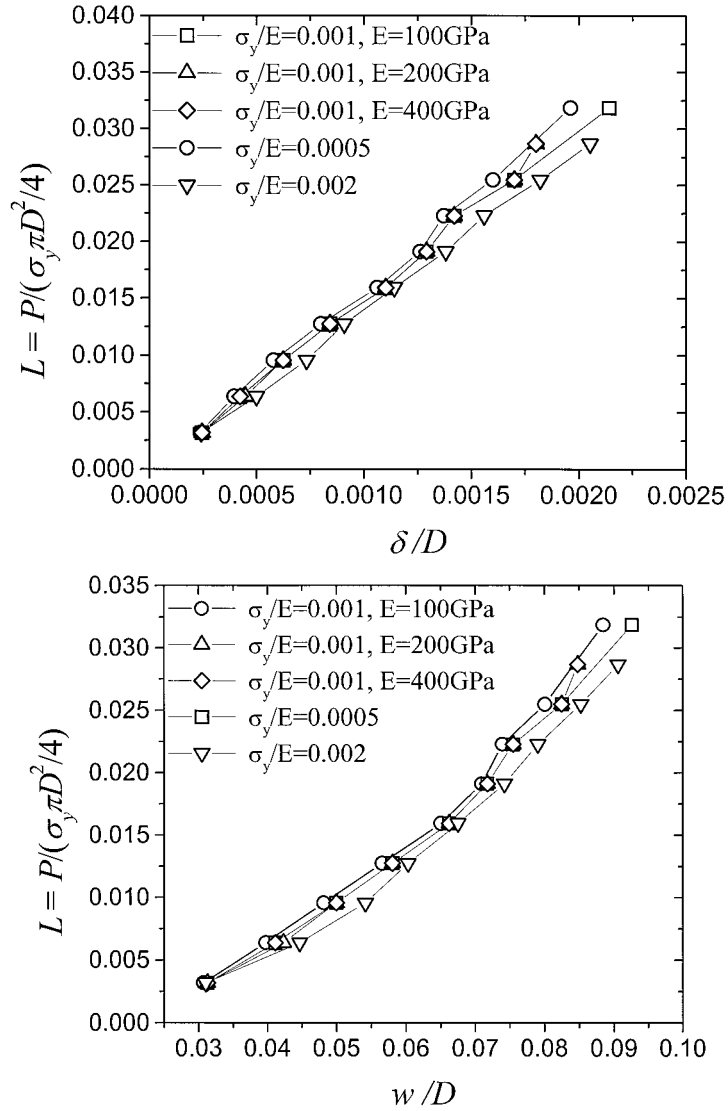
Figure 7. (a) L as a function of δ/D and (b) L as a function of w/D for different values of σ_y/E.
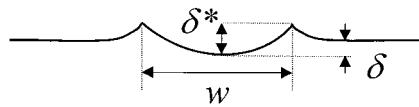

Figure 8. The pile-up that results in $\delta^* > \delta$.

outside the rim, $r > w/2$. Although there is some spread in the peak stresses just outside the rim, the stress distributions are roughly independent of L when the radial coordinate is scaled by the indent diameter w. Moreover, as seen in Figures 7a and 7b, the normalized indent depth δ/D and indentation diameter w/D vary with L in a manner that is essentially independent of σ_y/E. The fact that σ_y/E has little effect on these relations can be understood by noting that L in the moderately shallow indentation regime far exceeds the load levels for Hertzian indentation. Thus the elastic modulus plays essentially no role in these relations.

The relation between L and δ/D is nearly linear in Figure 7a, while that between L and w/D in Figure 7b is nearly parabolic. Given that both relations are essentially independent of σ_y/E and μ (see below), they are well approximated by

$$L \cong 15\frac{\delta}{D}, \tag{3}$$

$$L \cong 2.9(w/D)^2 \quad \text{or} \quad P \cong 2.3\sigma_y w^2. \tag{4}$$

With reference to Figure 8, note the difference between the two depth quantities, δ and the pile-up height $\delta*$. As has been noted elsewhere (Begley et al., 1999), $\delta* = \frac{1}{4}w^2/D$ holds in the shallow regime. But from the relations in (3) and (4), $\delta \cong 0.19\frac{w^2}{D}$. As seen in Figure 8, the difference in these two quantities is explained by the pile-up the indenter has caused in the elastic-perfectly plastic substrate.

From (3) and (4), the plastic work, PW, stored in the substrate is

$$PW = \int P \, \mathrm{d}\delta \cong 5.9\sigma_y D\delta^2 \cong 0.23\sigma_y \frac{w^4}{D} \tag{5}$$

This formula will be useful in making connection between the static indentation problem and the dynamic FOD problem discussed in the next section.

The results presented thus far for the stresses and deformation of the substrate have all been computed with the Coulomb friction taken to be $\mu = 0.1$. Many of these same computations have been repeated with $\mu = 1$. While the stresses within the rim of the indent do depend fairly strongly on the friction coefficient, the stresses outside the rim and the dependencies on L shown in Figure 7 differ only slightly for these rather extreme choices of the friction coefficient. For practical purposes these relations can be taken to be independent of μ for moderately shallow indents. Thus, the normalized hoop stress outside the rim is reasonably well approximated by

$$\frac{\sigma_{\theta\theta}(r, z)}{\sigma_y} = f_{\theta\theta}\left(\frac{r}{w}, \frac{z}{w}\right) \quad \text{when} \quad r > w/2 \quad \text{and} \quad 0.006 < L < 0.4, \tag{6}$$

where from (4) $w \cong 0.66\sqrt{P/\sigma_y}$ and the contour plot in Figure 4b gives $\sigma_{\theta\theta}$ for moderately shallow indentation. Most importantly, the indentation diameter w is the only quantity needed in scaling the stresses in this regime.

2.3. Plastic work of indentation and impact kinetic energy

Equation (5) gives the plastic work of indentation under conditions of quasi-static loading. In order to transfer the quasi-static results to the FOD problem, the fraction of the impact kinetic energy of the particle that is converted to plastic work must be known. To facilitate the transference, a plot of normalized plastic work as a function of normalized contact size w/D is given in Figure 9. The approximated formula, (5), can be used to determine this relation for moderately shallow indents, but the curve in Figure 9 is based on the finite element results in order to provide maximum accuracy. In addition, these results are extended into the deep indentation regime. Two impact points from the experimental results of Peters et al. (2000) are included in Figure 9 with the kinetic energy of the impacting particle replacing the plastic
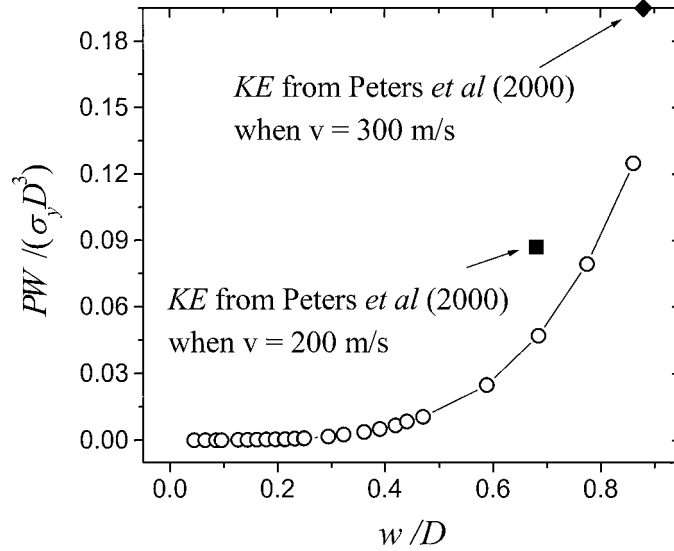
Figure 9. The normalized plastic work as a function of the normalized contact diameter. The total kinetic energy and resulting indent diameter of the impacting sphere for two of the tests of Peters et al. (2000) is also shown.

work in the vertical coordinate. Some of the details of the experiments (Peters et al., 2000) are as follows.

A hardened steel ball was used as the foreign object, with $D = 3.175mm$. The density of the steel is $\rho = 7.9\ Mg\ m^{-3}$. The yield stress of the substrate material (Ti-6Al-4V) is about $\sigma_y = 950\ MPa$. The impact velocity of the foreign object was in the range $v = 200$–$300\ \mathrm{m\ s^{-1}}$. The normalized kinetic energy of the foreign object, which was plotted in Figure 9, is:

$$\frac{KE}{\sigma_y D^3} = \frac{1}{12}\frac{\pi\rho D^3 v^2}{\sigma_y D^3} = \frac{\pi\rho v^2}{12\sigma_y}. \tag{7}$$

For an impact velocity $v = 200\ \mathrm{m\ s^{-1}}$, the experiment has $KE/\sigma_y D^3 = 0.087$ and $w/D = 0.68$, while the quasi-static analysis result at the same w/D has $PW/\sigma_y D^3 = 0.047$. This comparison suggests that 46% of the kinetic energy was dissipated by means other than plastic deformation of the substrate. Similarly, when $v = 300\ \mathrm{m\ s^{-1}}$, $KE/\sigma_y D^3 = 0.195$, $w/D = 0.88$, $PW/\sigma_y D^3 = 0.125$, implying that 36% of the kinetic energy was lost.

The 'lost energy' during impact may take the forms of the kinetic energy of the ricocheting particle, elastic waves in the substrate, and deformation energy in the particle. Assuming that all the lost energy is tied up in rebound kinetic energy, then by simple calculation for the shot with $v = 200\ \mathrm{m\ s^{-1}}$ in experiment (Peters et al., 2000), the steel ball should bounce back with a velocity $v' = 135\ \mathrm{m\ s^{-1}}$; and for $v = 300\ \mathrm{m\ s^{-1}}$, $v' = 180\ \mathrm{m\ s^{-1}}$. The explicit measured rebound velocities were not obtained.

In conclusion, the relation between normalized plastic work and contact diameter in Figure 9 for the quasi-static indentation, together with the experiments cited above, can be used to estimate the size of the indent and the associated stresses in the FOD problem. Specifically, assume the plastic work is about 60% of the kinetic energy of the FOD particle, and use Figure 9 to obtain w/D. The other characteristics of the damage then follow. The conversion factor, 60%, for the kinetic energy relies on only two data points, and more data will be required to establish the reliability of this factor.

After unloading, there are
3 most likely crack locations:
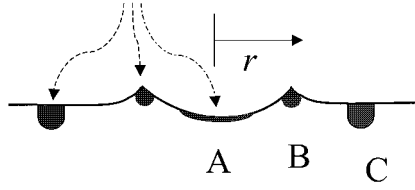$r = 0, r = w/2$ and $r \cong w.$

Figure 10. The three most likely crack locations.

3. Surface crack in residual stress field of the indent

The theoretical stress distributions indicate three possible regions where the residual stresses may enhance crack growth and lower the threshold of a surface crack. These regions where the hoop stresses are tensile, which have already been identified in Section 2, are designated by A, B, C in Figure 10. For very shallow indentations, from Figure 4a, there are only 2 hoop stress peaks: one at the bottom of the indentor at A and one at the crater ridge at B. The second peak in very shallow indentation is much larger than the first one, and it splits into peak B and peak C when L passes into the moderately shallow indentation regime. As L is increased within the moderately shallow indentation regime, the tensile peak at A becomes larger, while the stresses at B and C remain nearly the same, which can also be seen from Figure 5. For deep indentations, however, the peak at A has gone, only peaks B and C remain, with the stress at B being much larger than that at C. This can also be seen in Figure 5.

In this study we have focussed on moderately shallow indents and we will restrict our attention to small surface cracks centered at the peak hoop stress at C, which lies close to the point $r \cong w$. The emergence of surface cracks at the other two peaks will be explored in future work, but within this regime, it appears that C should be the critical point. There is a large compressive region directly beneath point A, which would tend to prevent a crack from propagating much below the surface. The peak at B is narrow compared with that of C, so the largest possible residual stress influence is expected for a crack centered at C.

The two tests referred to above (Peters et al., 2000) gave rise to fatigue crack initiation and growth from A for moderately shallow indent lying close to the deep indent transition, and from B for the case of a deep indentation. Thus, it will be important to explore crack growth from points A and B, as well, but the principles are illustrated by cracks placed at C.

Let a be the radius of a semi-circular surface crack centered at the peak of the hoop stress distribution at C, which roughly corresponds to the point $r = w$. Let K_{res} be the maximum value of the mode I stress intensity factor around the circumference of the crack. The residual stresses scale with and thus K_{res} will scale with $\sigma_y \sqrt{a}$. A three-dimensional finite element program (ABAQUS) has been used to compute the distribution of the stress intensity factor around the crack edge for many values of a/w and a number of values of the load parameter L. Because the indents were moderately shallow, the slight effect of the non-planarity of the surface was neglected in these computations, i.e., the surface of the substrate was taken to be planar. The calculation was performed by applying the residual hoop stress as computed in Section 2 to the faces of the crack. At each crack size, K_{res} was determined. The location along the circumference of the semi-circular crack where the maximum value of the mode I stress
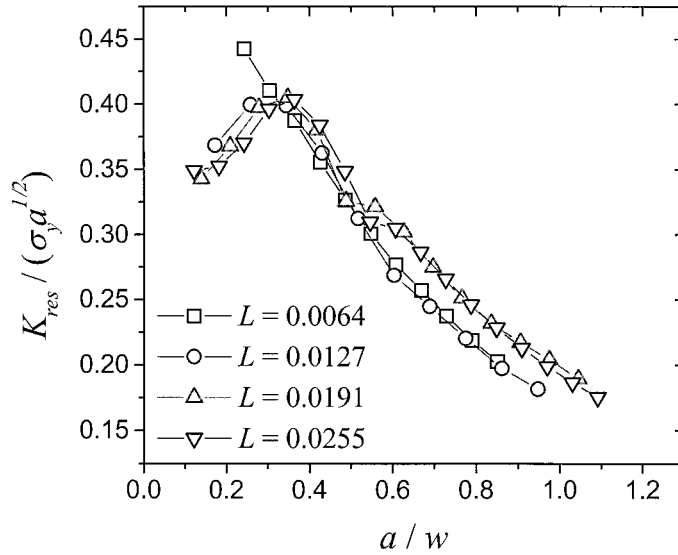
Figure 11. The normalized residual stress intensity factor $K_{res}/(\sigma_y\sqrt{a})$ as a function of a/w for moderately shallow indents.
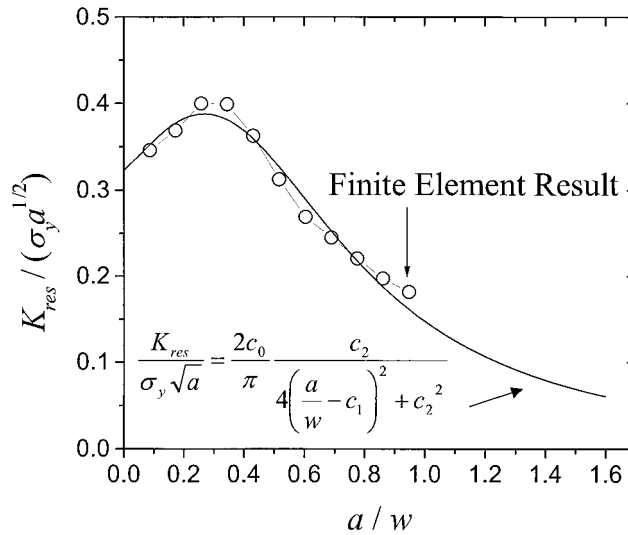

Figure 12. The functional fit between $K_{res}/(\sigma_y\sqrt{a})$ and a/w, which is independent of L in the moderately shallow indentation.

intensity factor (i.e., K_{res}) occurs is somewhere between the surface and depth, where the crack front is opened by the maximum residual hoop stress inside the substrate (cf., Figure 4 (b)). Computed curves of $K_{res}/\left(\sigma_y\sqrt{a}\right)$ as a function of a/w are presented in Figure 11 at four values of the load parameter, all of which lie within the moderately shallow indentation regime. The near-independence of these curves on L is tied to the fact that that normalized residual stresses discussed in Section 2 are also independent of L in this regime.

For the purposes of the subsequent fatigue crack analysis, a relatively simple functional form to represent the curves in Figure 11 was found with adjustable parameters chosen to give

the best fit.

$$\frac{K_{\text{res}}}{\sigma_y \sqrt{a}} = \frac{2c_0}{\pi} \frac{c_2}{4\left(\frac{a}{w} - c_1\right)^2 + c_2^2} \tag{8}$$

where $c_0 = 0.697$, $c_1 = 0.269$, $c_2 = 1.143$. This function is included in Figure 12. From (8), the maximum value of K_{res} (which is attained when $a \cong 0.4w$) is

$$(K_{\text{res}})_{\text{max}} = 0.24\sigma_y \sqrt{w}. \tag{9}$$

The role of the diameter of the indentation, w, is evident in this formula. Another important specialization of (8) pertains to the limit when the crack is small compared to the diameter of the indent ($a/w \to 0$). Then,

$$K_{\text{res}}^L = 0.32\sigma_y \sqrt{a}. \tag{10}$$

This result is simply that for a small semi-circular crack in a uniform stress field, $\sigma_{\theta\theta} = 0.24\sigma_y$, corresponding to the local stress at point C of the indent.

4. Fatigue crack threshold analysis in the presence of fod

4.1. SPECIFICATION OF THE CYCLIC LOADING AND STRESS INTENSITY HISTORY

The last step in the approach is to consider the combined effect of the residual FOD stresses and cyclic stresses on a pre-existing surface crack of radius a, as depicted in Figure 2. Specifically, the effect of the FOD damage on threshold growth conditions for the crack will be addressed. Given a cyclic loading history $\sigma(t)$, the following notation is used:

$$\begin{aligned} \sigma_{\text{max}} &\equiv \text{Max}\,[\sigma(t)] \\ \sigma_{\text{min}} &\equiv \text{Min}\,[\sigma(t)] \end{aligned} \quad ; R_{\text{applied}} = \sigma_{\text{min}}/\sigma_{\text{max}}. \tag{11}$$

By combining the contributions from the residual hoop stress and $\sigma(t)$, one obtains the total stress intensity factor on the semi-circular fatigue crack as

$$K(t, a) = K_{\text{res}}(a) + c \cdot \sigma(t)\sqrt{4a/\pi}, \tag{12}$$

where $c \cdot \sigma(t)\sqrt{4a/\pi}$ is the stress intensity factor of the semi-circular crack due only to $\sigma(t)$. For a full circular crack in an infinite body, $c = 1$. Based on the present finite element calculations for the semi-circular crack, we take $c = 1.2$. The total stress intensity factor range is therefore

$$\Delta K(a) \equiv \text{Max}(K(t, a)) - \text{Min}(K(t, a)) = (\sigma_{\text{max}} - \sigma_{\text{min}}) \cdot c \cdot \sqrt{4a/\pi}. \tag{13}$$

The total R-factor is

$$R(a) \equiv \frac{\text{Min}(K(t, a))}{\text{Max}(K(t, a))} = \frac{K_{\text{res}}(a) + c \cdot \sigma_{\text{min}}\sqrt{4a/\pi}}{K\text{res}(a) + c \cdot \sigma_{\text{max}}\sqrt{4a/\pi}} > R_{\text{applied}}. \tag{14}$$

Thus, as (13) emphasizes, ΔK is independent of the residual stress, however, from (14) is seen that the residual stress influences the R-factor in such a way that it is always larger that the
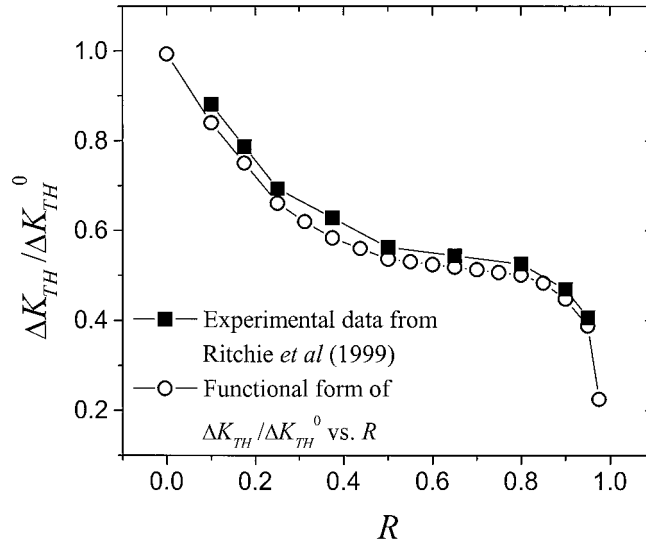
Figure 13. The $\Delta K_{TH}/\Delta K_{TH}^0$ vs. R data for Ti-6Al-4V (Ritchie et al., 1999) and a functional fit.

R-factor computed from the cyclic loads alone. To understand how FOD influences the fatigue behavior for a given material, one must consider the interplay between ΔK and R.

4.2. R-dependence of crack growth threshold data

As already mentioned, the emphasis here will be on the effect of FOD on fatigue crack growth threshold. To perform the analysis one must have fatigue crack data characterizing the curve of ΔK_{TH} versus R corresponding to threshold growth conditions. A convenient reference value for normalization purposes is

$$\Delta K_{TH}^0 \equiv \Delta K_{TH}\,(R = 0) \tag{15}$$

Complete threshold data are not available for many materials, but a reasonably complete set is available for the blade alloy of particular interest here, Ti-6Al-4V (Ritchie et al., 1999). These data are shown in Figure 13. For analysis purposes it is convenient to have a functional form for ΔK_{TH} vs. R. The function used here was obtained as a polynomial fit to the data. The cubic form

$$\frac{\Delta K_{TH}}{\Delta K_{TH}^0} = 1 - 2.49R + 4.78R^2 - 3.12R^3 \tag{16}$$

describes the data reasonably well. The limit of ΔK_{TH} when $R \to 1$ is unimportant, since the total R-factor will never approach that limit during this study.

4.3. Critical crack radius and an illustrative example

A given surface crack (with radius a) at the indentation is below threshold for a given cyclic loading if its associated ΔK and R calculated from (13) and (14) lie below the curve of ΔK_{TH} versus R. The critical crack radius at threshold, a_c, corresponds to

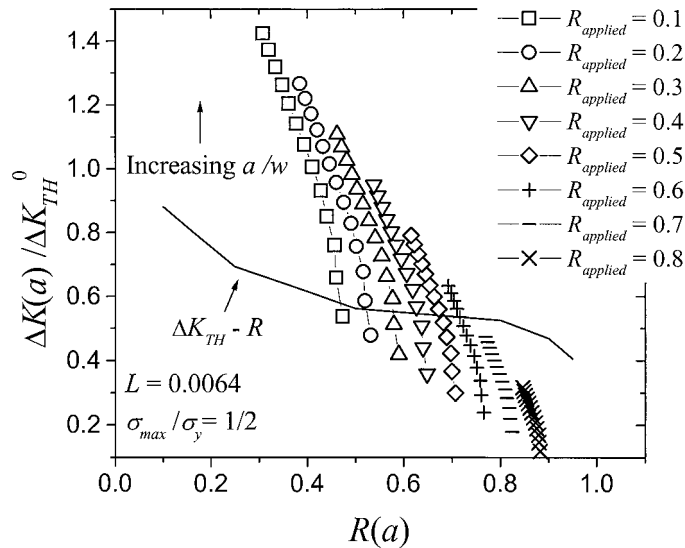$$\Delta K(a_c) = \Delta K_{TH} \quad \text{at} R(a_c) \tag{17}$$

Figure 14. $\Delta K(a)/\Delta K_{TH}^0$ vs. R (a) relations for $L = 0.0064$ and $\sigma_{max}/\sigma_y = \frac{1}{2}$, for various values of $R_{applied}$. For each of these curves corresponding to a particular $R_{applied}$, a/w increases from 0.12 at the bottom of the curve to 0.85 at the top. The points shown correspond to twelve equal increments in a/w. The critical value of a/w corresponds to the intersection with the curve for the threshold data.

The actual process of determining a_c is shown in Figure 14 for an indent with $L = 0.0064$ and $\sigma_{max}/\sigma_y = \frac{1}{2}$. Take as an example the loading with $R_{applied} = 0.5$. The sequence of points forming the curve of $\Delta K(a)/\Delta K_{TH}^0$ versus $R(a)$ correspond to increasing values of a/w starting from 0.12 at the lower end to 0.85 at the upper end. This curve cuts the crack
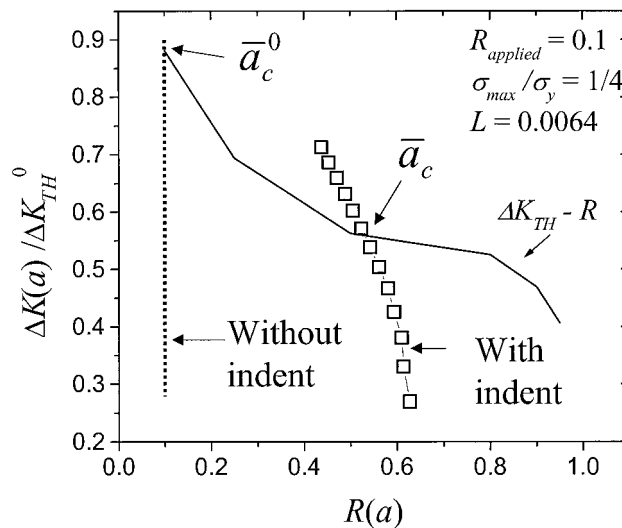

Figure 15. Illustration of the effect of residual stresses on the critical crack radius. In this case $L = 0.0064$, $\sigma_{max}/\sigma_y = \frac{1}{4}$ and $R_{applied} = 0.1$. The dotted vertical line is the relation $(\Delta K(a), R(a))$ in the absence of an indent with a increasing from bottom to top. The critical values of a correspond to the points of intersection with the threshold data.

growth threshold curve at $a_c/w = 0.39$. The sequence of points for the other values of R_{applied} can be interpreted in the same way. Note that for this example, loadings for which R_{applied} is equal to or greater than 0.7 have a critical crack radius lying beyond the range considered. To see the role of the residual stress of the indent more clearly, curves of $(\Delta K(a), R(a))$ for a particular loading are shown in Figure 15 for the substrate with and without an indent. Define the normalized critical crack radius as

$$\bar{a}_c = \frac{a_c}{(\Delta K_{TH}^0/\sigma_y)^2}. \tag{18}$$

In the absence of an indent, R is independent of a and intersects the threshold curve at $\bar{a}_c^0 = 7.60$. For the crack at the indent, the residual stress shifts the curve of $(\Delta K(a), R(a))$ significantly to the right and produces the variation of R with a given by (14). The normalized critical crack radius is $\bar{a}_c = 2.97$ (corresponding to $a_c/w = 0.52$). For this particular example, which has a relatively low value of R_{applied}, the critical crack size for the FOD damaged substrate is about 60% smaller than that for the undamaged substrate.

4.4. ANALYTICAL PROCEDURE FOR CRITICAL CRACK SIZE PREDICTION

The equations governing the stress intensity from the residual stress and from the cyclic loading are now put into another dimensionless form well suited to obtaining general results for the dependence of critical crack size on the various parameters of the FOD problem. With the normalized crack radius and indentation diameter defined by

$$\bar{a} = \frac{a}{(\Delta K_{TH}^0/\sigma_y)^2} \quad \text{and} \quad \bar{w} = \frac{w}{(\Delta K_{TH}^0/\sigma_y)^2}. \tag{19}$$

Equation (8) can be rewritten as

$$\frac{K_{\text{res}}}{\Delta K_{TH}^0} = \sqrt{\bar{a}}\frac{-2c_0}{\pi}\frac{c_2}{4\left(\frac{\bar{a}}{\bar{w}} - c_1\right)^2 + c_2^2} \equiv \sqrt{\bar{a}}f\left(\frac{\bar{a}}{\bar{w}}\right). \tag{20}$$

Substitution of this equation into (14) gives the total load ratio as a function of $\bar{a}$:

$$R(\bar{a}) = \frac{\sqrt{\bar{a}}f\left(\frac{\bar{a}}{\bar{w}}\right) + c\frac{\sigma_{\min}}{\sigma_y}\sqrt{\frac{4\bar{a}}{\pi}}}{\sqrt{\bar{a}}f\left(\frac{\bar{a}}{\bar{w}}\right) + c\frac{\sigma_{\max}}{\sigma_y}\sqrt{\frac{4\bar{a}}{\pi}}}, \tag{21}$$

with $c = 1.2$. By (13) and (16), the overall stress intensity factor range ΔK and the threshold ΔK_{TH} can both be represented as functions of $\bar{a}$ according to:

$$\frac{\Delta K(\bar{a})}{\Delta K_{TH}^0} = \frac{\sigma_{\max}}{\sigma_y}\left(1 - R_{\text{apply}}\right)c\sqrt{\frac{4\bar{a}}{\pi}} \equiv Q(\bar{a}), \tag{22}$$

$$\frac{\Delta K_{TH}}{\Delta K_{Th}^0} = 1 - 2.49R(\bar{a}) + 4.78R^2(\bar{a}) - 3.12R^3(\bar{a}) \equiv T(R(\bar{a})). \tag{23}$$

Therefore, the criterion to determine the critical crack radius at threshold, $\bar{a} = \bar{a}_c$, is simply
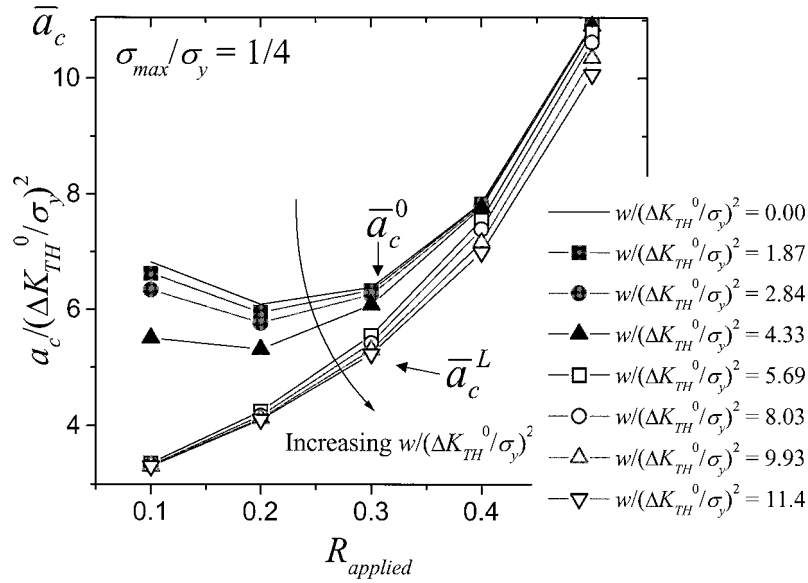
$$Q(\bar{a}_c) = T(R(\bar{a}_c)). \tag{24}$$

Figure 16. The normalized critical crack threshold $\bar{a}_c$ predicted from (24) as a function of R_{applied}, for a range of indentation sizes $\bar{w}$ with $\sigma_{\max}/\sigma_y = \frac{1}{4}$.

Based on the above equations, curves of normalized critical crack radius, $\bar{a}_c$, versus R_{applied} for $\sigma_{\max}/\sigma_y = \frac{1}{4}$ have been plotted in Figure 16 for a sequence of values of the normalized indentation diameter, $\bar{w}$. The plot brings out a clear transition from a critical crack radius $\bar{a}_c^0$ that is independent of $\bar{w}$ (and is the same as for a substrate with no FOD) to a lower limiting critical radius, $\bar{a}_c^L$, which is also essentially independent of $\bar{w}$. The range of the indention diameter over which the transition occurs corresponds roughly for $\bar{w}$ between 2 to 5. In other words, for this case with $\sigma_{\max}/\sigma_y = \frac{1}{4}$, indents smaller than about $\bar{w} = 2$ will have little influence on the critical crack size, while indents larger than about $\bar{w} = 5$ will result in a reduced critical crack radius $\bar{a}_c^L$ which is insensitive to even larger indents, as long as those indents remain in the moderately shallow regime.

The transition in $\bar{w}$ from essentially no effect due to FOD, to the reduced critical crack size is a strong function of $\sigma_{\max}/\sigma_y$. Calculations similar to those described above have been performed for other values of $\sigma_{\max}/\sigma_y$, and the transition range is plotted in Figure 17.

4.5. LIMITING CRITICAL CRACK SIZE

The limiting critical crack radius, a_c^L, corresponds to the limit $a/w = \bar{a}/\bar{w} = 0$ in (20), such that $f(a/w) = 0.32$. The resulting equations for a_c are independent of w. In this limit, the indent is sufficient large (but still not deep!) such that the critical crack at C is embedded in a locally uniform residual stress corresponding to $\sigma_{\theta\theta} = 0.24\sigma_y$. The effect of the residual stress on the total stress intensity factor comes in solely through the elementary result given in (10). It follows that the prediction for the limiting critical crack radius due to moderately shallow indents can be carried out directly using (10) together with (13) and (14).

Consider the implications for two materials given $\sigma_{\max}/\sigma_y = \frac{1}{4}$. For Ti-6Al-4V ($\sigma_y = 950$ MPa and $\Delta K_{TH}^0 = 5$ MPa $\sqrt{m}$ (Ritchie et al., 1999)), the transition indentation diameter
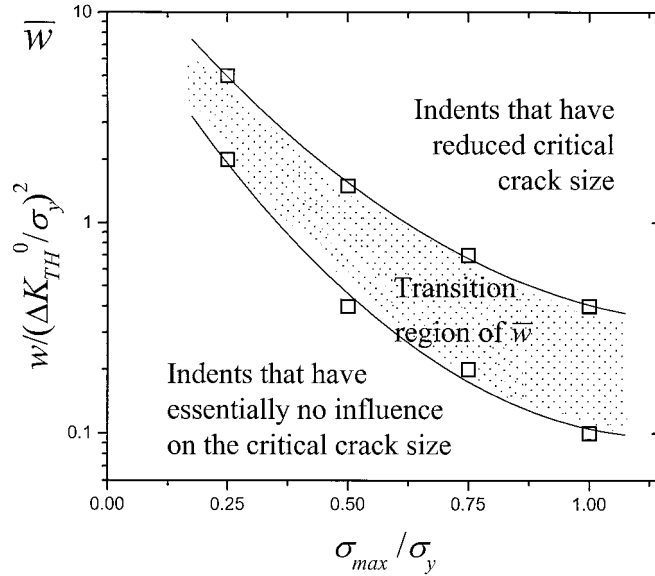
Figure 17. Transition range of normalized indentation size as a function of σ_{max}/σ_y for moderately shallow indents. Indents below the transition have essentially no influence on the critical crack size, while indents above have the reduced critical crack size.
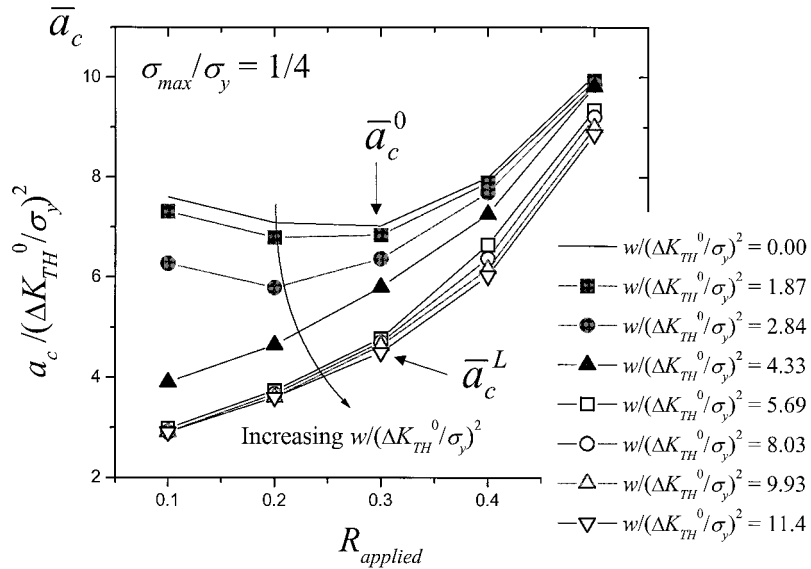

Figure 18. The normalized critical crack threshold $\bar{a}_c$ computed from full finite element result as a function of $R_{applied}$, for a range of indentation sizes $\bar{w}$ with $\sigma_{max}/\sigma_y = \frac{1}{4}$.

($\bar{w} = 2$) is about $w = 0.05$ mm. If $R_{applied}$, then $a_c^L = 0.09$ mm, which can be compared with $a_c^0 = 0.2$ mm for no FOD. Clearly, a very small FOD will have an effect on the critical crack threshold for this particular material. By contrast, for mild steel which has a lower yield stress and a higher threshold, ($\sigma_y = 200$ MPa and $\Delta K_{TH}^0 = 15$ MPa $\sqrt{m}$), and the transition occurs at a much larger indent diameter, $w = 11$ mm. Now, for $R_{applied} = 0.1$, one obtains $a_c^L = 18$ mm, which can be compared with $a_c^0 = 43$ mm for no foreign object damage.

5. Accuracy of the analytical formulation and further results

The analysis underlying the plots in Figure 16 relies on the accuracy of the formula (20) for the effect of the residual stress on the stress intensity factor of the surface crack. Formula (20) has been obtained by fitting the finite element results over a range of the load parameter L within the moderately shallow regime. Outside this regime (20) loses accuracy. The smallest indents in Figure 16 (those with $\bar{w} = 2\text{--}4$) are very shallow such that the accuracy of these curves is suspect. The results of Figure 16 have been recalculated using the full finite element determination of K_{res}, without recourse to the approximation (20), and therefore valid for all L. The plot from the full finite element calculation is shown in Figure 18. These are again for the case $\sigma_{\text{max}}/\sigma_y = \frac{1}{4}$ and can be compared directly with the previous plots based on the approximate formula (20) in Figure 16. While there is some discrepancy between the two plots for the smaller values of $\bar{w}$, the characterization of the transition by $2 < \bar{w} < 5$ remains robust. Moreover, the limiting value of the reduced critical crack radius, a_c^L, is unchanged because the indent size associated with this limit is within the regime of moderately shallow indents. The same remarks apply to the results for the other values of $\sigma_{\text{max}}/\sigma_y$, for which the transition range of the indentation size has been given in Figure 17. In conclusion, even though (20) loses accuracy for very shallow indents, the consequences for the predictions of the transition from essentially no effect due to FOD to a reduced critical crack size is relatively minor.

A comparison is made in Figure 19 between the normalized critical crack radius in the absence of any indent, $\bar{a}_c^0$, and the normalized limiting critical crack radius, $\bar{a}_c^L$, for moderately shallow indents is made for a wide range of loadings. The normalized critical crack radius is plotted versus the applied load ratio R_{applied}, for four values of $\sigma_{\text{max}}/\sigma_y$. The curves in Figure 19a are obtained from full finite element simulations, while those in Figure 19b make use of the analytic approximation (20) for K_{res}. As already anticipated, the analytical approximation is highly accurate for determining $\bar{a}_c^L$. Over much of the cyclic loading space, $\left(\sigma_{\text{max}}/\sigma_y, R_{\text{applied}}\right)$, the effect of moderately shallow indents is relatively small in that $\bar{a}_c^L$ is only slightly below the critical crack radius with no indent $\bar{a}_c^0$. However, large effects of the indent on reducing the critical crack size occur at high values of R_{applied} and also at low values of R_{applied} when $\sigma_{\text{max}}/\sigma_y$ is small.

6. Conclusion

Fracture due to foreign object damage is a rather new topic, which brings together contact mechanics, crack mechanics and fatigue analysis. In this paper, finite element methods have been used to investigate the residual stresses due to a spherical indentation and their influence on the stress intensity of a surface crack emerging at a critical location at the indent. A complete framework has been established to analyze the effect of the residual stresses on the crack growth due to subsequent cyclic loading. In particular, the critical crack size associated with threshold fatigue crack growth has been emphasized. While detection of cracks of the critical size may be extremely difficult, or even impossible in high strength materials, the fact that the critical crack size is reduced by FOD is in itself useful knowledge.

The work presented here is just a beginning in that it has primarily focussed on a limited range of indentations, referred to here as being moderately shallow. In addition, attention has been directed to surface cracks emerging from only one location just outside the indent.
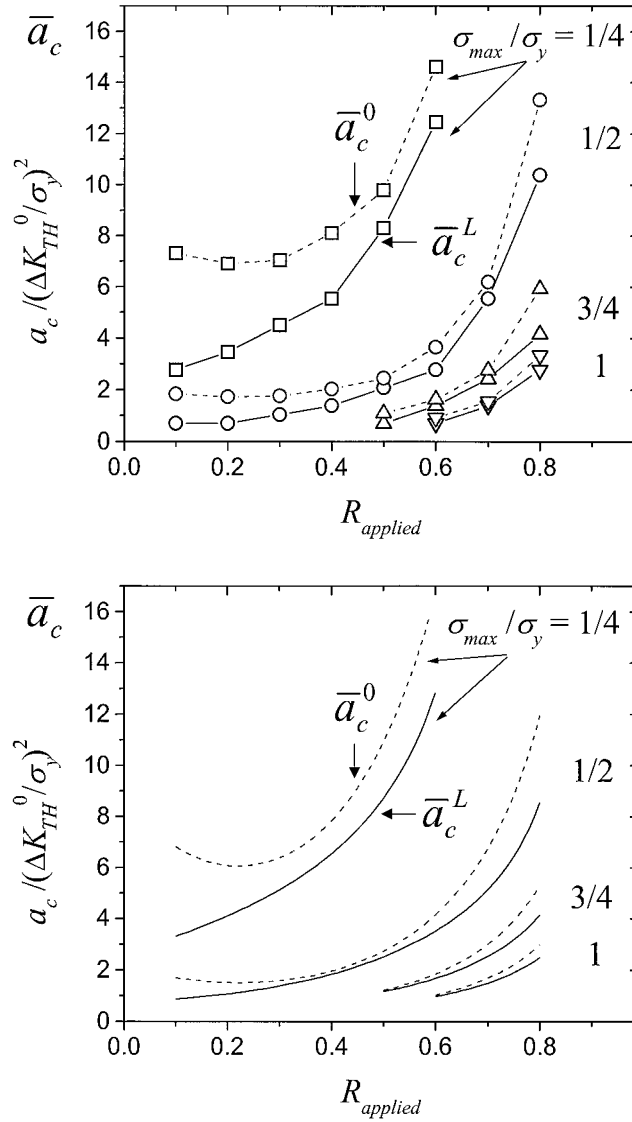
Figure 19. The normalized critical crack radius for shallow indentation, $\bar{a}_c^0$ for no indents and $\bar{a}_c^L$ for sufficiently large indents, for a range of R_{applied} and $\sigma_{\mathrm{max}}/\sigma_y$ values. (a) full finite element result, (b) analytical result from (24).

Experimental observations suggest that other locations may be equally, or even more, critical in deeper indentations. Subsequent work will be needed to extend these findings in both directions. We conclude by listing the main findings and implications of the current research:

1. Three indentation regimes were identified with distinct residual stress patterns: very shallow, moderately shallow and deep indents. The present paper focused primarily on the moderately shallow regime corresponding to $0.006 < L < 0.4$, where $L = P / \left(\frac{1}{4} \pi D^2 \sigma_y \right)$ is the load parameter. The friction coefficient μ and the elastic yield strain, σ_y/E, have minor influence on the residual tensile hoop stress. Estimates for the load factor and the depth of penetration in terms of the kinetic energy of an impacting sphere are given.

2. For moderately shallow indents, the effect the residual stress on a surface crack located just outside the indent (point C in Figure 10) has been determined and an accurate analytic approximation for the stress intensity factor has been presented.

3. The combination of cyclic fatigue loading and the residual stress due to the FOD for fatigue crack growth has been explored, with emphasis on the largest (critical) crack size that remains below the fatigue crack growth threshold. For cracks at moderately shallow indents, FOD can reduce the critical crack size by as much as 60%, depending on the cyclic loading history. The non-dimensional parameter controlling the reduction of the critical crack size is $\bar{w} = w/(\Delta K_{TH}^0/\sigma_y)^2$, where w is the diameter of the indent and ΔK_{TH}^0 is the stress intensity variation at $R = 0$ associated with threshold crack growth in the material. When $\sigma_{\max}/\sigma_y = \frac{1}{4}$, for values of $\bar{w}$ less than about 2, the indent has little effect on the crack growth threshold; for values of $\bar{w}$ greater than about 5, the full reduction in the critical crack size is attained. Similar results have been given for other values of $\sigma_{\max}/\sigma_y$ (cf., Figure 17).

Acknowledgements

References

Begley, M., Evans, A.G. and Hutchinson, J.W. (1999). Spherical impression of thin elastic films on elastic-plastic substrates. *International Journal of Solids and Structures*, submitted.

Biwa, S. and Storakers B. (1995). Ananalysis of fully plastic Brinell indentation. *J. Mech. Phys. Solids* **43**, 1303–1334.

Bower, A.F., Fleck, N.A., Needleman, A. and Ogbonna, N. (1993). Indentation of power law creeping solids. *Proceeding Royal Society of London* **A441**, 97–124.

Hibbit, Karlsson & Sorensen Inc. (1998). *ABAQUS version 5.7 User's Manual*, Hibbit, Karlsson & Sorensen Inc., Pawtucket, RI.

Hill, R., Storakers, B. and Zdunek, A.B. (1989). A theoretical study of the Brinell hardness test. *Proceedings Royal Society of London* **A423**, 301–330.

Johnson, K.L. (1985). *Contact Mechanics*, Cambridge University Press, Cambridge.

Mesarovic, S.D. and Fleck, N.A. (1999a). Spherical indentation of elastic-plastic solids. *Proceeding Royal Society London*, in press.

Mesarovic, S.D. and Fleck, N.A. (1999b). Frictionless indentation of dissimilar elastic-plastic spheres. *International Journal of Solids and Structures*, in press.

Peters, J.O., Roder, O., Boyce, B.L., Thompson, A.W. and Ritchie, R.O. (2000). Role of Foreign Object Damage on Thresholds for High-Cycle Fatigue in Ti-6Al-4V. *Metallurgical and Materials Transactions A*, in review.

Ritchie, R.O., Davidson, D.L., Boyce, B.L., Campbell, J.P. and Roder, O. (1999). High-Cycle Fatigue of Ti-6Al-4V. *Fatigue and Fracture of Engineering Materials and Structures* **22**, 621–631.